44th AIAA Aerospace Sciences Meeting and Exhibit
9 - 12 January 2006, Reno, Nevada

AIAA 2006-1401

Adaptive Control of Separated Flow

Ye Tian* and Louis N. Cattafesta III†
Department of Mechanical and Aerospace Engineering
University of Florida, Gainesville, FL, 32611
Rajat Mittal‡
Department of Mechanical and Aerospace Engineering,
The George Washington University
Washington DC, 20052

Adaptive closed-loop control is used to optimize the lift-to-drag ratio of post-stall separated flow over a NACA 0025 airfoil using multiple amplitude-modulated (AM) or burst-modulated (BM), zero-net-mass-flux (ZNMF) actuators that cover the central 33% span of the airfoil. A simplex optimization approach uses the lift and drag measured by a strain-gauge balance for feedback and searches for the optimal AM or BM actuation parameters in a closed-loop fashion. An energy penalty function based on the electrical power consumption of the actuators is added to the cost function to study the tradeoff between the aerodynamic performance and the power requirement. In the baseline post-stall separated flow over the airfoil, two dominant characteristic frequencies are identified via flow visualization and hot-wire anemometry: the convective instability of the separated shear layer and the global instability of the vortex shedding in the wake. Closed-loop control increases the lift-to-drag ratio by a factor of 2-3 via small-amplitude AM and BM forcing of nonlinear interactions between these instabilities.

I. Introduction

Flow separation is the breakaway or detachment of flow from a solid surface. It incurs a large amount of energy/lift loss and limits the performance of many flow-related devices (e.g., airplanes, diffusers, etc.). Researchers have sought to eliminate or at least mitigate flow separation for over a century because of its large potential payoff in many applications. Recent efforts using periodic, as opposed to steady, excitation have demonstrated the ability to attach separated flow efficiently (e.g., Greenblatt and Wygnanski 2000).

Leading-edge shear layer rollup and vortex shedding in the wake are two characteristic features of post-stall flow (Wu et al. 1998). Huerre and Monkewitz (1990) suggest that this type of shear flow (with a pocket of absolute instability of sufficient size) may display intrinsic dynamics of the same nature as in a closed-flow system. Therefore, it is reasonable to postulate that separated flow over an airfoil acts as a nonlinear multi-frequency closed-flow system (Mittal et al. 2005). In such a system, the shear layer instability (with characteristic frequency f_{SL}) and

* Graduate Research Assistant, yetian@ufl.edu, Student Member AIAA.
† Associate Professor, cattafes@ufl.edu, Associate Fellow AIAA.
‡ Associate Professor, mittalr@gmail.com, Associate Fellow AIAA.

the global wake instability (with vortex shedding frequency f_{wake}) may interact with each other in a nonlinear fashion. The present study is focused on how this system responds to small amplitude-modulated (AM) (Wiltse and Glezer 1993) or burst-modulated (BM) (Amitay and Glezer 2002), zero-net mass-flux (ZNMF) forcing targeted at these instabilities.

Although numerous studies are reported in the literature to determine the optimal forcing frequencies for effective separation control, the observed values of optimal F^+ vary over a wide range. For example, Greenblatt and Wygnanski (2000) concluded that the optimal range is $2 < F^+ < 4$. Seifert and Pack (1999) found that the excitation frequency should be chosen such that $0.5 < F^+ < 1.5$ over a wide range of high Reynolds numbers. Conversely, Amitay et al. (2001) found that when the excitation frequency $F^+ > 10$, the lift-to-pressure-drag ratio was larger than when the excitation frequency $F^+ < 4$ for their unconventional airfoil.

This study attempts to explore this controversy and determine optimal forcing schemes by utilizing a quasi-static, adaptive closed-loop control approach. The approach implements a simplex optimization algorithm (Press et al. 1992) and uses the measured lift and drag forces for feedback and ZNMF actuators. An energy penalty function based on the electrical power consumption of the actuators is added to the cost function to consider the tradeoff between aerodynamic performance and power requirements. The outline of the paper is as follows. Section II summarizes the experimental configuration and setup, while Section III describes the feedback control algorithm. Section IV presents experimental results, and Section V offers conclusions and discusses future work.

II. Experimental Configuration

A NACA 0025 airfoil with a 15.24 cm chord and 30.48 cm span serves as the test model in a low speed wind tunnel facility with a 30.48 cm square test section. The nominal Reynolds number based on chord length is $\mathrm{Re}_c = 10^5$. The angle of attack for this study is 20º. The BL is tripped at the leading edge using sand grit.

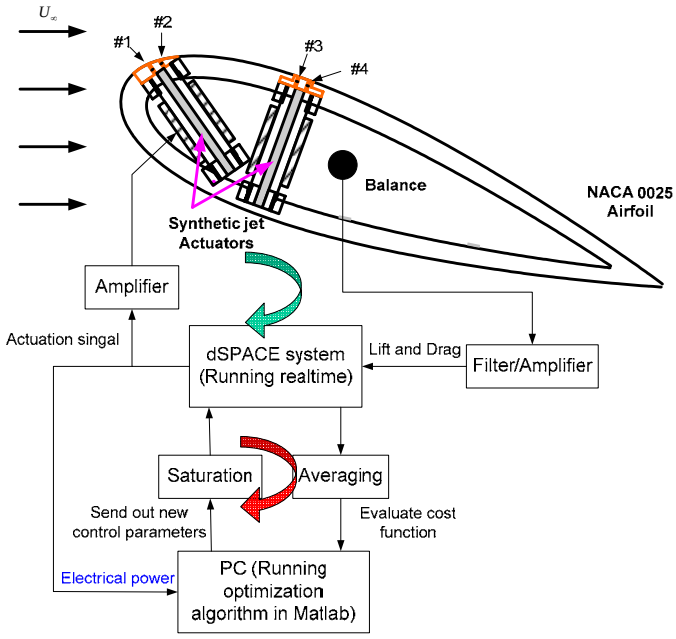

Figure 1: Experimental configuration.

As shown in Figure 1, the airfoil is fitted with four ZNMF actuators, all of which are located in the central 33% spanwise region of the airfoil and have $h = 0.5$ mm wide slots. The first two (#1 and #2) are located near the leading edge of the airfoil at approximately 3% chord and are separated by 2.4 mm, while an identical second pair (#3 and #4) is placed near the point of maximum thickness at approximately 30% chord. Gallas et al. (2003) describe the design of the actuators. For this study, only the first actuator pair is used because it is closest to the separation point for the chosen flow conditions. The slots of unused actuators are covered.

A balance is used to measure the lift and drag forces of the airfoil. Several pairs of strain gauges are attached to a cantilevered, annular shaft that supports the isolated airfoil to measure the lift, drag, and pitching moment (not used in this study). The estimated uncertainty of the force balance is 7 mN, which corresponds to an uncertainty of ±0.0025 in lift and drag coefficients at the current test conditions.

As shown in Figure 1, dual-timing control loops are configured to implement the optimization algorithms (described in Section III). The first loop synchronously controls the actuators and measures the low-pass filtered and amplified balance signal, while the second loop averages the balance output and performs optimization in an asynchronous fashion. The second loop acts as a supervisory controller that updates the control parameters in the first loop. The sampling rate of the first loop is 40 kHz, while the second loop runs on a host PC at O(Hz). The first-loop is implemented by a dSPACE (Model DS1005) DSP system with 466MHz PowerPC CPU and 16-bit A/D and D/A boards. The optimization algorithm is programmed in Matlab and communicates directly with the dSPACE system to adjust the actuator signal.

The electrical power consumption of the actuator is defined as $V_{rms} I_{rms}$, where V_{rms} and I_{rms} are the root-mean-square values of the voltage and the current of the actuator, respectively. The current is measured by a Tektronix (Model TCP A300) current sensor. The electrical power of the actuator is used by the optimization algorithm to impose a penalty function based on power consumption.

A Dantec constant-temperature, hot-wire anemometry system (CTA module 90C10) is used to acquire instantaneous velocity data. Before the experiments, a calibration is performed by the calibration module and the flow unit (90H01 and 90H02). A 5 μm hot wire probe (55P11) is mounted on a 2-dimensional Velmex traversing system with approximately 1.6 $\mu m / step$ spatial resolution in both directions. The velocity data were sampled at 10.24 kHz by a 16-bit dynamic signal acquisition system, and the alias-free frequency span was set to 4 kHz.

Flow field visualization and quantitative velocity data over the surface of the airfoil and in the wake are acquired using Particle Image Velocimetry (PIV). The PIV system consists of two 15 Hz, 50 mJ per pulse, Nd:YAG lasers with appropriate light sheet optics and a TSI model 630157 Powerview Plus 2MP (1600 x 1200 pixels) 10-bit CCD camera.

III. Control Algorithm

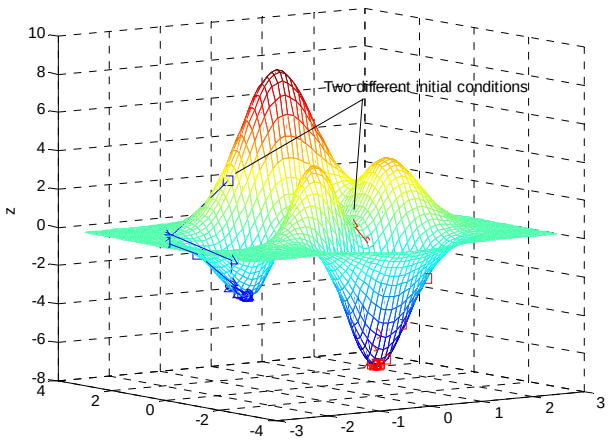

Figure 2: Simulation results of downhill simplex algorithm.

Various optimization strategies are discussed in the literature (Press et al. 1992). After some experimentation with various extremum-seeking algorithms (Artiyur and Krstic 2003; Banaszuk et al. 2003), the downhill simplex method was implemented to minimize the drag-to-lift ratio. The benefits of the algorithm are its simplicity and applicability to multi-parameter optimization. The key steps of the algorithm are summarized as follows: 1) evaluate the cost function at chosen initial conditions, 2) use the lowest value as reference and search for a lower value of the cost function, 3) move only in the downhill direction, and 4)

terminate when some convergence criteria are met.

The performance of the downhill simplex algorithm is illustrated for 2-dimensional simulation case (Figure 2). The cost function is obtained in Matlab by the "peaks" command. The formula for the cost function is as follows:

$$Z = 3[(1-x)^2 - (y+1)^2] - 10(x/5 - x^3 - y^5)e^{-x^2-y^2} - e^{-(x+1)^2-y^2}/3 \quad (1)$$

This function has two local minima and a global minimum. As shown in Figure 2, the optimization algorithm converges to either a local minima or the global minimum depending on the initial condition. This is dictated by the inherent "downhill" nature of the algorithm. To increase the probability of finding the global minimum, numerous initial conditions are used.

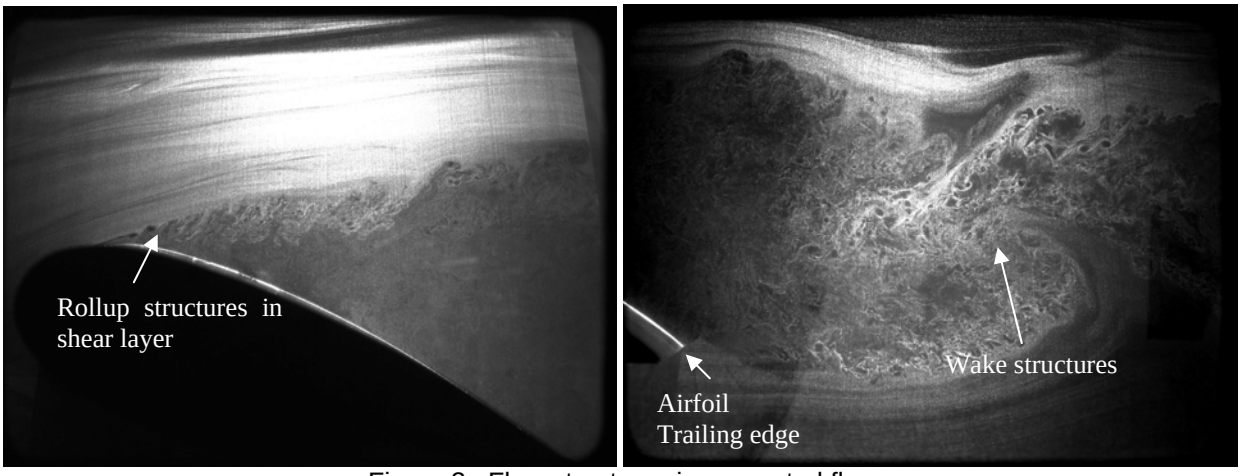

Figure 3: Flow structures in separated flow.

IV. Results

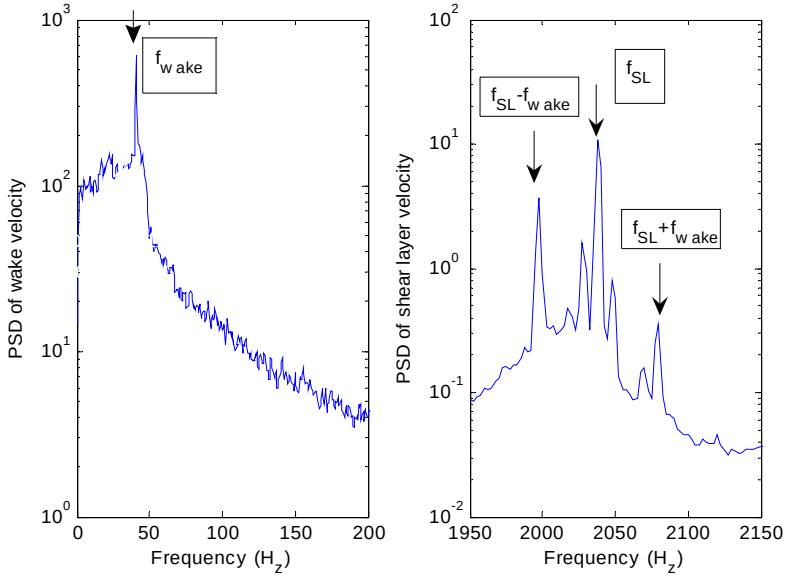

Figure 4: Wake (1 chord aft of TE) and shear layer (near separation) power spectral density at peak rms location.

Post-stall flow is characterized by leading-edge shear layer rollup and vortex shedding in the wake as shown in Figure 3. The flow will likely be governed by nonlinear interactions between these instabilities (Mittal et al. 2005).

Figure 4 shows a plot of the u_{rms}^2 power spectral density of the wake and the shear layer at the respective peak RMS locations for the baseline, uncontrolled flow obtained with a hot-wire probe. The wake spectral density is obtained 1 chord

aft of the trailing edge, while the shear layer spectral density is obtained near the separation location. The PSD was estimated using a 4096 point FFT, a Hanning window with 75% overlap, and 100 blocks. The plots zoom in on two interesting regions. The left plot clearly shows the dominant wake frequency f_{wake}. The right plot provides evidence for the nonlinear coupling between the shear layer and wake instabilities via the presence of the shear layer frequency f_{SL} and the sum/difference frequencies $f_{SL} \pm f_{wake}$. Note that f_{SL} is much higher than f_{wake} in accordance with classical scaling arguments that $f_{SL} \sim U_\infty / \theta_{sep}$ and $f_{wake} \sim U_\infty / W_{wake}$. Based on the definition $F^+ = f X_{TE} / U_\infty$, $f = f_{SL}$ gives $F^+ \sim O(30)$ and $f = f_{wake}$ give $F^+ \sim O(1)$. Thus, more than a single characteristic frequency exists, perhaps explaining the wide range of effective forcing frequencies reported in the literature.

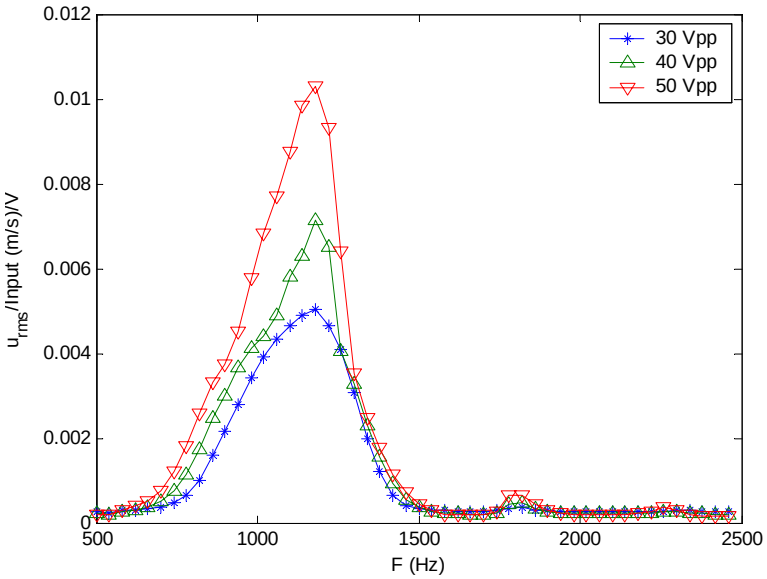

Figure 5: Frequency response of ZNMF actuator 1.

As suggested by Wiltse and Glezer (1993), amplitude modulation is used as the excitation signal of the ZNMF actuators to produce sufficient output at off-peak frequencies. In this study, amplitude modulation takes the following form:

$$e(t) = A \sin\left(2\pi f_c t\right) \frac{1 + \sin\left(2\pi f_m t\right)}{2}$$

where A is the amplitude, f_c is the carrier frequency (usually the resonant frequency of the actuator) in Hz, and f_m is the modulation frequency (which is also the targeted frequency in the flow) in Hz.

As an example, the frequency response to sinusoidal excitation, i.e., rms velocity/voltage, of actuator #1 is plotted in Figure 5. The peak output occurs at approximately 1200 Hz, and significant output is apparently limited to a bandwidth of 500-1500 Hz, precluding the possibility of directly forcing the low-frequency wake instabilities via sinusoidal excitation. Furthermore, the nonlinear nature of the actuators is revealed, since the frequency response function is not independent of the input voltage. It is this nonlinear behavior that is leveraged to enable forcing at low and high frequencies, as explained below.

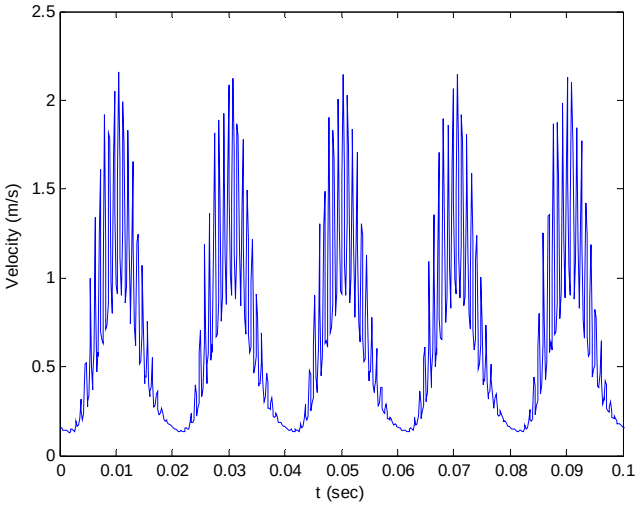

Figure 6: Measured response (via hot-wire anemometry) to AM excitation of the ZNMF actuator.

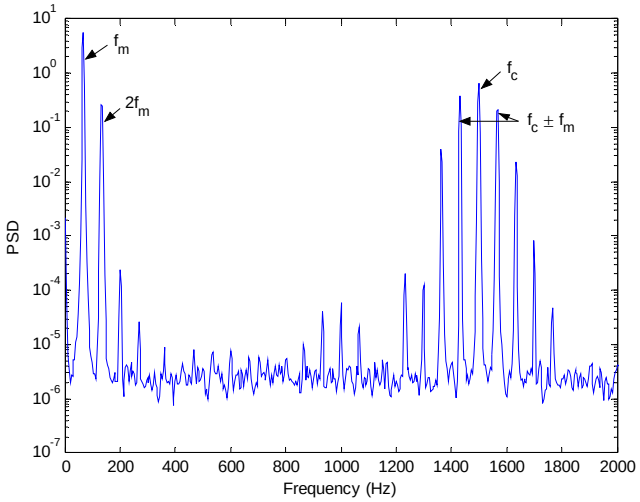

Figure 7: Power spectral density of the AM hot-wire velocity signal shown in Figure 6.

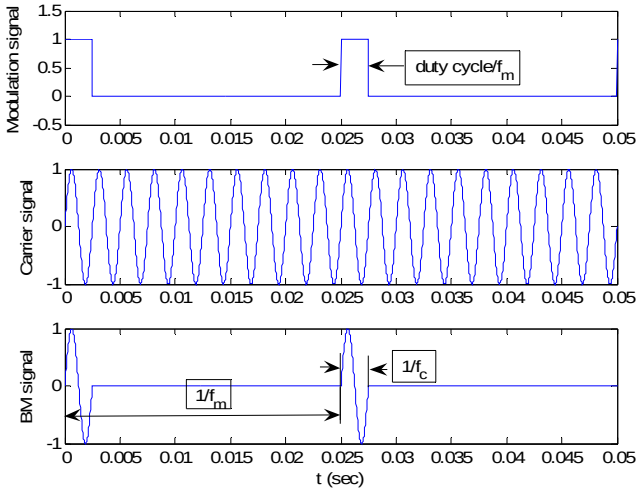

Figure 8: BM signal demonstration.

Figure 6 shows the output of the ZNMF actuator measured by the hot-wire anemometry subject to an AM excitation, where $A = 50$ V_{pp}, $f_m = 50$ Hz and $f_c = 1180$ Hz. The wire was place at a distance above the actuator slot so that there is no reverse flow and, hence, no signal rectification is needed. The corresponding power spectrum of the AM signal shown in Figure 7 reveals the low frequency output at 50 Hz is much larger than can be obtained via sinusoidal excitation at 50 Hz. This shows that the actuator demodulates the AM signal due to the nonlinear nature of the system. Amplitude modulation thus allows an actuator operating at or near its resonant frequency to generate significant disturbances at characteristic frequencies of the flow that are far from the nominal bandwidth of the device.

Another type of actuation signal has been suggested by Amitay and Glezer (2002), and these authors call this "pulse modulation". This waveform is generated by modulating a sine wave by a square wave with an adjustable duty cycle. We term this type of the actuation signal "burst modulation" to be consistent with standard function generator terminology. In this study, the duty cycle is varied so that the signal contains a single cycle of the sine wave in each pulse. The parameters to be optimized are again the amplitude, f_m and f_c. Figure 8 demonstrates how the BM signal is generated. The carrier signal ($f_c = 400\ Hz$ sine wave) is multiplied by the modulation signal ($f_m = 40\ Hz$ square wave) to generate the periodic BM signal.

Closed-loop control experiments have been carried out using the downhill simplex algorithm. AM and BM excitation are used for the first pair of actuators. The goal is to search for optimal A, f_c, and f_m to minimize the drag-to-lift ratio using various initial conditions. Amplitude and frequency

range limits are employed to protect the actuator as well as to concentrate on interesting regions.

First, simple one-dimensional optimization (i.e., optimize only one parameter while others are fixed) is carried out using the AM signal. The results are obtained by starting from several different initial conditions. The results reveal that A always converges to the maximum limit for both of the actuators. When actuator #1 is operated alone, the modulation frequency f_m converges to $\sim(2 \text{ to } 4)\, f_{wake}$, while f_c is fixed at the peak response frequency of the actuator shown in Figure 5. Table 1 summarizes the optimization results. Alternatively, the carrier frequency f_c converges to the vicinity of $f_{SL}/2$, corresponding to sub-harmonic forcing of the shear layer, when f_m is fixed at 80 Hz ($2 f_{wake}$). Table 2 summarizes the optimization results. Note that, in both cases, the lift-to-drag ratio, using only 33% span forcing, is increased by approximately a factor of 2.

Optimized f_m (Hz)	Optimized L/D (Baseline = 1.27)
153	2.57
95	2.56
120	2.44

Table 1: f_m optimization results for the actuator #1 with $A = 15\,V$ and $f_c = 1180\,Hz$.

Optimized f_c (Hz)	Optimized L/D
1040	2.65
1297	2.66
1250	2.44

Table 2: f_c optimization results for the actuator #1 with $A = 15\,V$ and $f_m = 80\,Hz$.

When actuator #2 is operated alone, the modulation frequency f_m converges to the same range as actuator #1 ($2 f_{wake} \sim 4 f_{wake}$). However, the carrier frequency f_c converges to the vicinity of the shear layer f_{SL} (1700 Hz ~ 2500 Hz). An interesting fact is that this range is far from the maximum response of the actuator (see Figure 5).

Figure 9, Figure 10, and Figure 11 show instantaneous smoke-flow visualizations of baseline and controlled cases by actuator #1 and #2, respectively. Interestingly, both actuators only partially reattach the separated flow. Further investigation is required to determine if this is an optimal result when seeking to maximize L/D or merely due to a limitation of the actuators.

The case in which two actuators are run simultaneously has also been studied. Since the optimal f_c of actuator #1 is ~1/2 of the optimal f_c of actuator #2, f_{c1} is constrained to be $\frac{1}{2} f_{c2}$. When f_{c2} converges to 2300 Hz, L/D converges to 2.74, which is an improvement compared to the single actuator cases at the expense of increased input power.

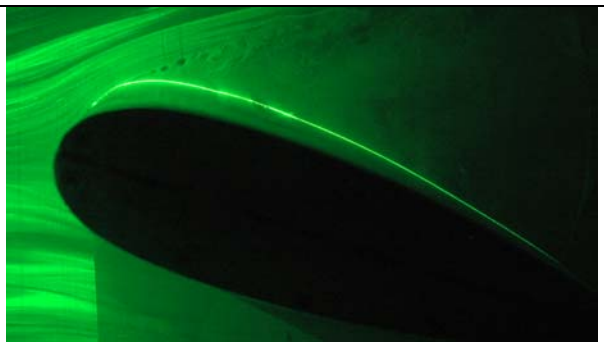

Figure 9: Flow visualization: baseline.

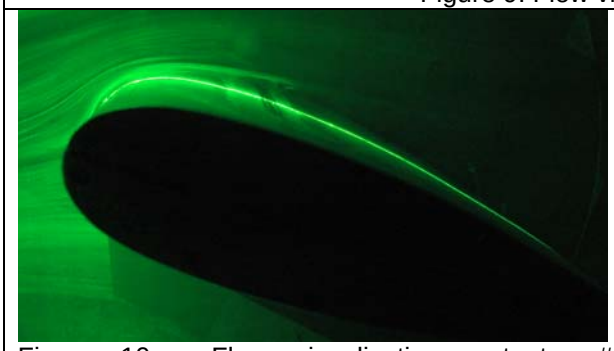

Figure 10: Flow visualization: actuator #1 operating at optimal conditions.

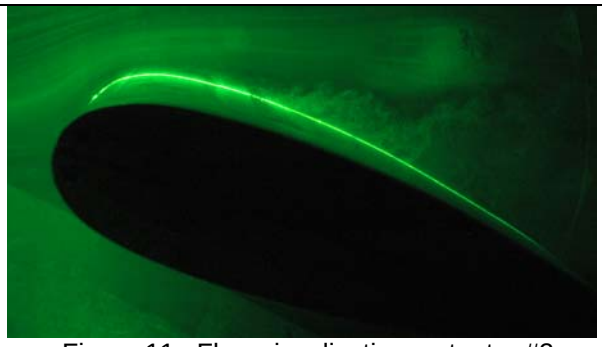

Figure 11: Flow visualization: actuator #2 operating at optimal conditions.

Next, three-dimensional optimization (i.e., A, f_m and f_c) is attempted using both AM and BM signals but only actuator #1. In addition, an energy penalty is also implemented. The overall dimensionless cost function consists of the sum of the drag-to-lift ratio and a normalized power: $f = \frac{D}{L} + W\frac{V_{rms}I_{rms}}{DU_\infty}$, where W is a weighting factor to balance the D/L and the energy penalty.

Table 3 summarizes the optimization results. Cases 1 and 3 are the results for AM and BM signals without power penalty, respectively. Then, *after the optimization algorithm is converged*, the power penalty is turned on (i.e., W=100), and the results are summarized as cases 2 and 4. The $c_\mu = u_{rms}^2 h / \left(0.5U_\infty^2 c\right)$ for each case is also estimated using the hot wire anemometer and is summarized in Table 3. The constraint on the amplitude of the excitation signal was 30 V_{pp}.

One can see that f_m and f_c converge to similar values as shown in Table 1 and Table 2. The optimization using an AM signal without energy penalty gives the best performance in terms of L/D. On the other hand, the optimization using a BM signal only slightly degrades L/D while requiring only about 11% of the power required by amplitude modulation. Another interesting point is that after the energy penalty is turned on, the algorithm is able to significantly reduce the power with only slight performance degradations.

Figure 13 to Figure 16 show the time-averaged velocity fields obtained using 300 PIV image pairs for the baseline case and the four cases in Table 3. The black line in the figures indicates the zero velocity contour and reveals the separation location. The separation is delayed by 43%, 33%, 33% and 30% chord length for cases 1, 2, 3 and 4, respectively. These results confirm the performance shown in Table 3.

Table 3: Optimization results for both AM and BM signals with and without energy penalty.

Converged Values	Case 1: AM (W=0)	Case 2: AM (W=100)	Case 3: BM (W=0)	Case 4: BM (W=100)
f_m (Hz)	78	55	80	93
f_c (Hz)	1040	1245	1250	1286
V_{pp}	30	6	30	10
overall cost function	0.39	0.43	0.42	0.45
L/D	2.56	2.38	2.38	2.27
normalized power	7×10^{-3}	1.4×10^{-4}	7.8×10^{-4}	1×10^{-4}
c_μ	1.72×10^{-4}	5.77×10^{-6}	1.17×10^{-5}	2.96×10^{-6}

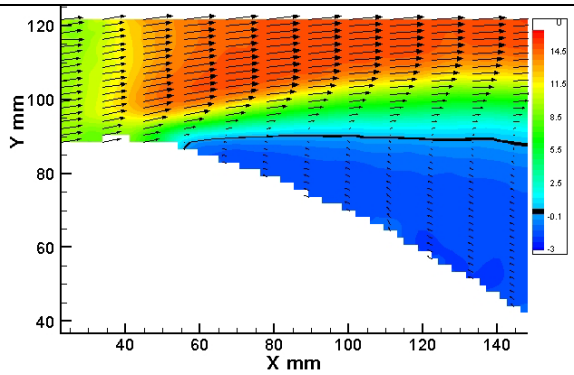

Figure 12: Flow velocity field for the baseline case (no control).

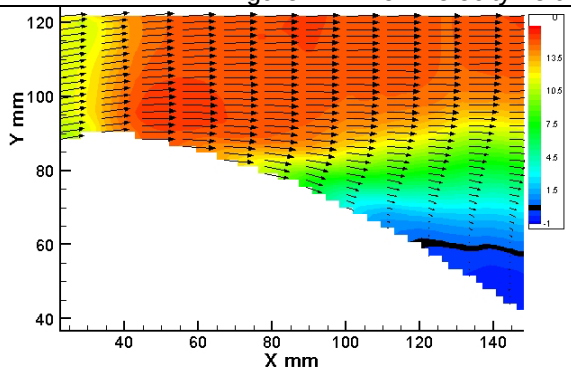

Figure 13: Flow velocity field for case 1.

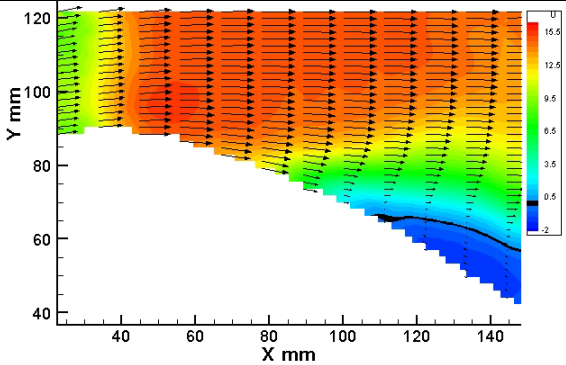

Figure 14: Flow velocity field for case 3.

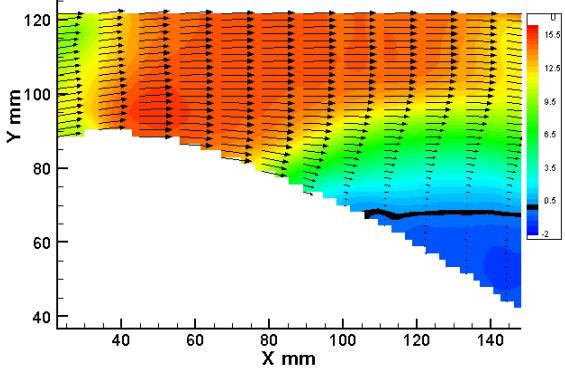

Figure 15: Flow velocity field for case 2.

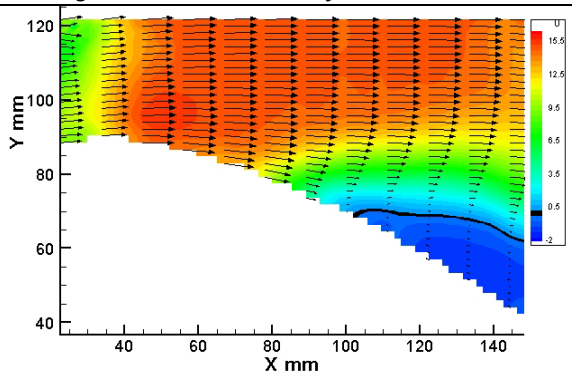

Figure 16: Flow velocity field for case 4.

V. Conclusions and Future Research

The flow over a NACA 0025 airfoil, at 20° angle of attack and $\mathrm{Re}_c = 100,000$, is separated at the leading edge. In the post-stall separated flow, there are two characteristic instabilities: the shear layer and wake instabilities. Experimental evidence has suggested that they are nonlinearly coupled. Both instabilities are important to control the separated flow via unsteady excitations.

A quasi-static, adaptive, nonlinear closed-loop control scheme for the separated flow has been developed to search for the optimal AM or BM actuation parameters using ZNMF devices. The downhill simplex algorithm is used as the optimization algorithm. The results seeking to maximize L/D with and without an energy penalty are promising and reveal the importance of forcing nonlinear interactions between the shear layer and wake instabilities. Furthermore, the importance of actuator dynamics is revealed. ZNMF actuators are nonlinear systems themselves. Their nonlinear characteristics add complexity but also enable forcing of instabilities with characteristic frequencies that are widely separated.

The BM actuation signal gives comparable performances while requiring less energy compared with the AM actuation signal. An energy penalty function based on the electrical power of the actuator is added to the cost function to consider the trade off between the aerodynamic performance and power requirements. The implementation of the energy penalty function is able to reduce the required power with only modest performance reductions for both AM and BM actuation signals. On the other hand, preliminary tests have shown that, when starting with a separated flow with the energy penalty function turned on, results in poorer aerodynamic performance. This highlights the differences between attaching a separated flow and keeping an attached flow from separating.

Future research includes detailed flow measurements using the hot-wire anemometry and PIV to understand what the effect of the control is on the flow. Furthermore, we plan to investigate other cost functions, besides D/L, that seek, for example, to maximize lift or minimize drag.

Acknowledgments

This work was supported by the Air Force Office of Scientific Research Grants FA9550-05-1-0093 and FA9550-05-1-0169, monitored by Dr. Rhett Jefferies.

References

Amitay, M, and Glezer, A., "Controlled transients of flow reattachment over stalled airfoils," *International Journal of Heat and Fluid Flow*, Vol. 23, pp. 690– 699, 2002.

Amitay, M., Smith, D., Kibens, V., Rarekh, D. and Glezer A., "Aerodynamic Flow Control over an Unconventional Airfoil Using Synthetic Jet Actuators," *AIAA Journal*, Vol. 39 No.3, March 2001, pp. 361-370.

Artiyur, K. B. and Krstic, M., Real-Time Optimization by Extremum-Seeking Control, Wiley-Interscience, 2003.

Banaszuk, A., Narayanan S. and Zhang Y., "Adaptive Control of Flow Separation in a Planar Diffuser," *AIAA paper 2003-0617*, 2003.

Greenblatt, D and Wygnanski, I, "The control of flow separation by periodic excitation," *Progress in Aerospace Sciences*, 36:487-545, 2000.

Griffin, B., Senior Thesis, University of Florida, 2003.

Hajj, M. R., Miksad, R. W. and Powers, E.J., "Perspective: Measurements and Analyses of Nonlinear Wave Interactions with Higher-Order Spectral Moments", *Journal of Fluids Engineering*, Vol. 119, Mar. 1997, pp. 3-13.

Holman, R., Quentin, G., Carroll, B. and Cattafesta, L., "Interaction of Adjacent Synthetic Jets in an Airfoil Separation Control Application", *AIAA paper 2003-3709*, June 2003, Orlando, FL.

Huerre, P. and Monkewitz, P., "Local and Global Instabilities in Spatially Developing Flows," *Annual Review Fluid Mechanics*, 1990. 22: pp. 473-537.

Kegerise, M. A., Spina, E. F., Garg, S. and Cattafesta, L., "Mode-Switching and Nonlinear Effects in Compressible Flow over a Cavity", *Physics of Fluids*, Vol. 16, No. 3, Mar. 2004, pp. 678 – 687.

Mittal, R., Kotapati, B. and Cattafesta, L., "Numerical Study of Resonant Interactions and Flow Control in a Canonical Separated Flow," *AIAA paper 2005-1261*, Reno, Nevada, Jan. 2005.

Press, W. H., Flannery, B. P., Teukolsky, S. A. and Vetterling, W. T., Numerical Recipes in Fortran, 2nd edition, January 1992, Cambridge University Press.

Gallas, Q., Holman, R., Nishida, T., Carroll, B., Sheplak, M., and Cattafesta, L., "Lumped Element Modeling of Piezoelectric-Driven Synthetic Jet Actuators," *AIAA Journal*, Vol. 41, No. 2, pp. 240-247, 2003.

Seifert, A., Pack, L. G., "Oscillatory Control of Separation at High Reynolds Numbers," *AIAA Journal*, Vol. 37, No.9, Sep. 1999, pp. 1062-1071.

Wiltse, J. N. and Glezer, A., "Manipulation of Free Shear Flows Using Piezoelectric Actuators," *Journal of Fluid Mechanics*, Vol. 249 pp. 261-285, 1993.

Wu, J. Z., Lu, X.Y., Denny, A.G., Fan, M. and Wu, J.M., "Post-Stall Flow Control on an Airfoil by Local Unsteady Forcing", *Journal of Fluid Mechanics*, Vol. 137, 1998, pp. 21-58.